X International Conference on Computational Methods in Marine Engineering
MARINE 2023
J. Garcia-Espinosa, L. González, J.E. Gutiérrez & B. Serván-Camas (Editors)

Dynamic Response of a Net Cage Induced by a Sudden Mooring Line Failure in Regular Waves and Currents

Hung-Jie Tang[1*], Ray-Yeng Yang[2] and Hao-Cheng Yao[2]

[1] Tainan Hydraulics Laboratory, National Cheng Kung University, 70955 Tainan, Taiwan.

[2] Department of Hydraulic and Ocean Engineering, National Cheng Kung University, 70101Tainan, Taiwan

[*] Corresponding author: Hung-Jie Tang, hjtang@thl.ncku.edu.tw

ABSTRACT

Over the recent two decades, despite the engineering technology of marine fish cages in Taiwan having been well-developed, incidents of mooring line failure still occur sporadically. Once successive failures of mooring happened, the entire mooring system will crash resulting in the net being entangled and structures being damaged. The massive number of farmed fish may die or escape, which not only brings enormous economic losses but also has an irreversible ecological impact. Therefore, this study aims to investigate the mechanism of mooring line failure on the net cage through model tests and numerical simulations. The influence of one mooring line failure on a net cage was studied by Tang et al. (2021). The influence of successive failures of two mooring lines on a net cage was studied by Tang et al. (2022a). Following the previous study, this study focuses on the influence of mooring line failure on the net cage under regular waves and currents. The results show that after the failure of the upstream mooring line, the tension in the remaining mooring line increases substantially. Both the experimental and numerical results show similar trends, that the maximum tension value after the failure increases with wave height and wave period.

Keywords: net cage; mooring line failure; model test; numerical simulation; dynamic response.

1. INTRODUCTION

Although the cage farming industry in Taiwan has developed well over the past two decades, mooring line failures are still a common occurrence (Tang et al., 2020). When a mooring line fails, the floating collars collide and the fish net becomes entangled. This often leads to a significant loss of farmed fish and the potential escape of fish from the cage, resulting in significant economic losses and incalculable ecological impacts. In addition, the development of cage farming in deeper waters is becoming increasingly necessary due to conflicts with other marine activities. Therefore, it is essential to study the failure of mooring lines in net cages caused by waves and currents in order to plan for future development.

In an effort to understand the mechanism of mooring line failure, many studies have been conducted in recent years. Yang et al. (2020) developed a time-domain numerical model to investigate the effect of mooring line failure on a net cage under various waves and currents. Tang et al. (2020) conducted research on the dynamic response of net cages subjected to irregular waves and currents caused by mooring line failure. Their results showed significant changes in the response spectra of both the wave and low frequency regions. They also conducted a laboratory experiment to verify their numerical model

for a net cage subjected to mooring line failure (Tang et al., 2021; Tang et al., 2023). Cheng et al. (2021) investigated the effect of mooring line breakage on the dynamic response of net cages exposed to currents. Their research showed that at current velocities less than 0.5 m/s, breakage of a mooring line is unlikely to cause immediate progressive collapse of the fish farm, but may result in structural collapse and fish escape as the current and waves increase. Hou et al. (2022) investigated the reliability of the mooring system of net cages with a damaged mooring line and showed that the failure of one mooring line significantly increases the probability of failure of the remaining mooring lines. Tang et al. (2022a) investigated the dynamic response of sequential mooring line failure in a net cage through numerical simulations and model tests. The results showed that the responses of mooring tension, cage motion, and remaining cage volume after the second failure were higher than after the first failure. Recently, Tang et al. (2022b) evaluated the two potential disasters of mooring line failure and anchor sinking with respect to seabed sand waves in an offshore wind farm area in Taiwan.

In this study, both model tests and numerical simulations were used to investigate the dynamic response of sudden mooring line failure on a net cage subjected to regular waves and currents. The study estimated the influence of mooring line failure on the adjacent line tensions and floating collar rotations by comparing it to the intact mooring condition. In addition, the influence of wave height and wave period on mooring line failure and floating collar rotation was determined by varying their values. The study also included a comparison of results between model tests and numerical simulations. The remainder of this paper is organized as follows: Section 2 described the model test; Section 3 introduced the numerical model; Section 4 compared the mooring tension and rotational motion under intact and failed states of the mooring and the influence of increasing wave height and wave period on the mooring line failure of a net cage in regular waves and currents; and Section 5 drawn conclusions and provides recommendations for future work.

2. MODEL TEST

2.1 Experimental setup

Figures 1 and 2 depict the net cage model used in this study, and Table 1 provides its specifications. The wave tank used in the experiment is 50 m in length, 7 m in width, and 1.2 m in depth. The model was placed approximately 30 m from the wave maker, 20 m from the end wall, and 3.5 m from the side wall. The wave and current directions were set to the x-axis direction, making the mooring system symmetrical to the environmental force. The full-scale net cage had a 30 m diameter inner floating collar and a 12.5 m deep net installed in water with a constant depth of 20 m. Froude scaling with geometric similarity was applied in the model test, with a scale of 1:25. Table 1 also presents the corresponding full-scale values, although replicating the geometric similarity, particularly the netting, was difficult. Therefore, the corresponding full-scale values in Table 1 are only provided for reference (Huang et al., 2006; Kristiansen and Faltinsen, 2015).

The net cage model used in the study consisted of a floating collar, net chamber, tube sinker, buoy, and mooring line attached to the bottom of the wave tank. Two load cells were attached to a plate on the tank wall and connected to two upstream mooring lines via pulleys. The load cells were type LT6-5 from SSK Company, Japan, with repeatability of 0.2% FS, linearity of 0.2% FS, temperature characteristics of 0.05% RO/°C, output voltage of ±10 V, input and output resistance of 500 Ω, and an operating temperature range of -15 to 75°C. The highest recorded force during the test was 49.05 N. An Xsens IMU (MTW2-3A7G6) was mounted on the edge of the floating collar to measure rotational motion. Three Nortek (Norway) ADVs were placed on the front of the net cage model to simultaneously

measure inflow velocity. The ADVs were evenly spaced 100 cm apart and the average of their readings was taken as the inflow velocity. Two LED markers were attached to the center of the floating collar and tube sinker to observe upwelling and downwelling motions, following Tang et al. (2022a). However, due to the sandy bottom and muddy water quality caused by wave generation, the image processing method was not applicable. Therefore, only rotational motion results were available for analysis.

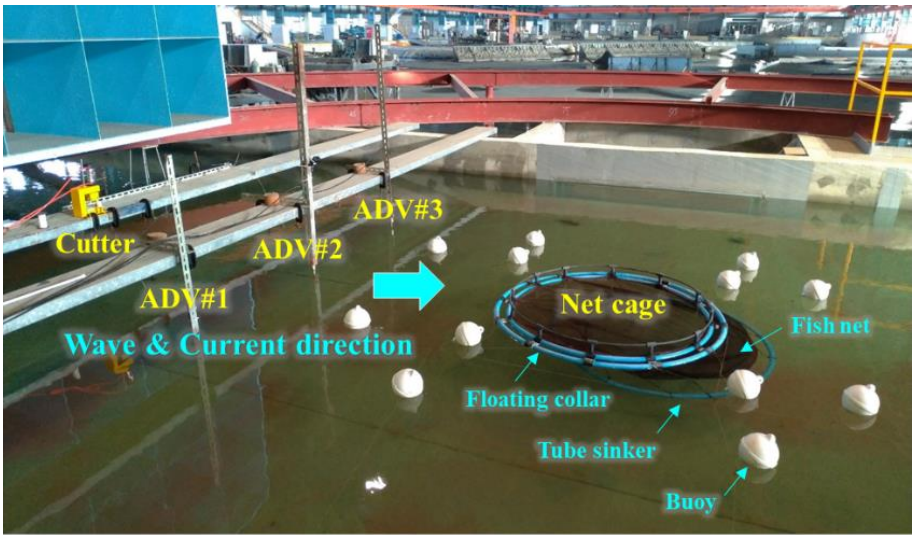

Figure 1. Photo of the net cage model installed in a wave tank.

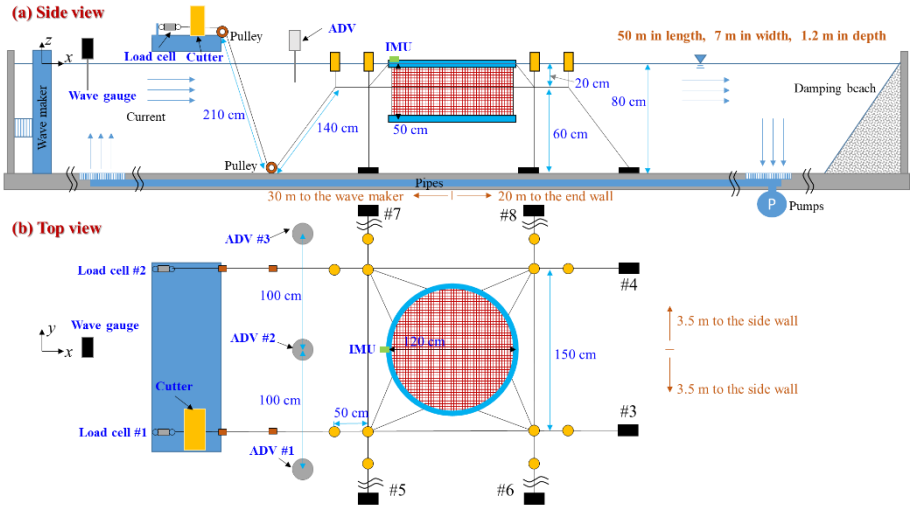

Figure 2. Schematic diagram of the model test.

Two methods presented in existing studies can induce mooring line failure in a laboratory environment. The first method is the use of the line cutting device (Figure 1) proposed by Tang et al. (2021). The device consists of a blade and a pneumatic cylinder that provides cutting force through an air compressor. The second approach is the electromagnet described by Tang et al. (2022a), which can be turned off to cut the mooring line. The first method is used here because the second method was proposed after this experiment.

Table 1. Specifications of the net cage model.

Component	Specification	Model scale	Full scale	Scale ratio
Floating collar	Inner circumference	377.0 cm	94.25 m	1:25
	Outer circumference	408.4 cm	102.1 m	1:25
	Tube diameter	3.4 cm	0.85 m	1:25
	Density	0.950 g/cm^3	950 kg/m^3	1:1
	Total mass	3,724 g	58,188 kg	1:25^3
	Total buoyancy	6,774 g	105,844 kg	1:25^3
Fish net	Twine diameter	0.02 cm	0.5 cm	1:25
	Mesh size	0.60 cm	15 cm	1:25
	Solidity	0.128	0.128	1:1
	Net depth	50 cm	12.5 m	1:25
	Density	1.14 g/cm^3	1140 kg/m^3	1:1
	Young's modulus	2.424 GPa	2.424 GPa	1:1
	Total mass	71.5 g	1,117 kg	1:25^3
Tube sinker	Circumference	408.4 cm	102.1 m	1:25
	Tube diameter	3.4 cm	0.85 m	1:25
	Total mass	1,320 g	20,625 kg	1:25^3
	Density	0.95 g/cm^3	950 kg/m^3	1:1
Mooring line	Diameter	0.265 cm	6.625 cm	1:25
	Unit mass	0.039 g/cm	2.437 kg/m	1:25^2
	Density	1.14 g/cm^3	1140 kg/m^3	1:1
	Young's modulus	0.753 GPa	0.753 GPa	1:1
Buoy	Diameter	15 cm	3.75 m	1:25
	Buoyancy	1,450 g	22,656 kg	1:25^3
	Total mass	230 g	3,594 kg	1:25^3

2.2 Experimental procedure

Figure 3 illustrates the test procedure. The no-load offset readings from the load cells, wave gauges, gyro and ADVs were first recorded. The pre-tensioning of the two mooring lines was then checked using the readings from two load cells and adjusting the difference between them to less than 5%. This was done to ensure that the forces in the mooring system were symmetrical. The current velocity was then increased to a predetermined value. The flow field was allowed to stabilize for 30 minutes. The regular wave was then generated by the wave maker. The steps that make up the main part of the experiment are presented here. First, the measurements from the load cells and the ADVs of the mooring system were collected for 60 s in the intact state. After 30 s, the button was pressed to cut the mooring line connected to load cell #1. The remaining recording time was 30 s (approximately 12 to 18 waves), which had been verified in the pre-test phase to be sufficient to capture the dynamic responses after the failure. The limited time is because the regular waves in the wave tank can cause wave reflections that must be taken into account. Finally, the test data was reviewed and the wave and current generators were stopped if found to be in order.

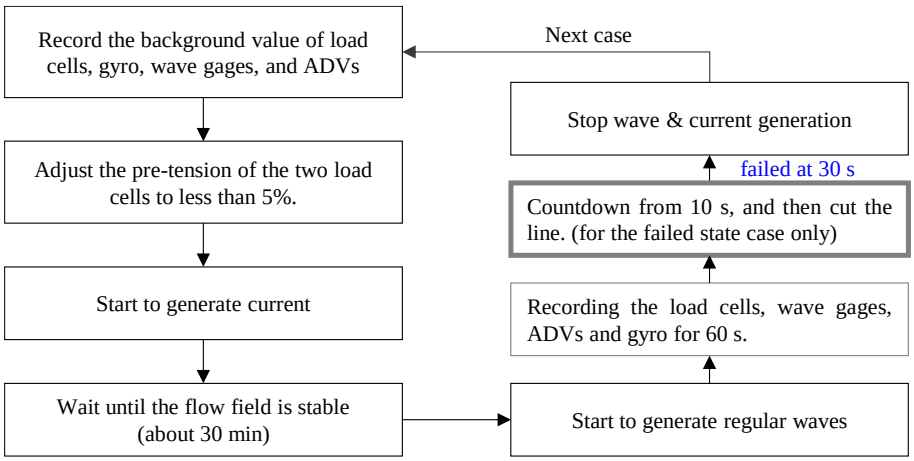

Figure 3. Flowchart of a single experimental case.

2.3 Test cases

Wave height and wave period are two main factors of the regular wave, they can lead to different dynamic responses to the floating structures. Thus, this study investigated the effects of wave heights and wave periods. Tables 2 and 3 show the test cases of five different wave heights with the same wave period and current velocity under the intact and failed mooring conditions, respectively. Similarly, Tables 4 and 5 illustrate the test cases of five wave periods with the same wave height and current velocity under the intact and failed mooring states, respectively.

Table 2. Test cases for different wave heights under intact mooring.

Test case	Wave height (cm)	Wave period (s)	Current velocity (cm/s)
RH1I	8.91	1.98	22.59
RH2I	13.10	1.99	22.59
RH3I	17.16	2.00	24.27
RH4I	21.32	2.00	22.21
RH5I	25.86	2.02	25.81

Table 3. Test cases for different wave heights under failed mooring.

Test case	Wave height (cm)	Wave period (s)	Current velocity (cm/s)
RH1F	8.49	1.98	22.59
RH2F	12.60	2.01	22.59
RH3F	16.49	1.98	24.27
RH4F	20.00	1.99	22.21
RH5F	24.43	2.01	25.81

Table 4. Test cases for different wave periods under intact mooring.

Test case	Wave height (cm)	Wave period (s)	Current velocity (cm/s)
RT1I	16.43	1.61	24.69
RT2I	17.98	1.80	23.84
RT3I	17.16	2.00	24.27
RT4I	15.42	2.22	25.41
RT5I	15.94	2.41	24.82

Table 5. Test cases for different wave periods under failed mooring.

Test case	Wave height (cm)	Wave period (s)	Current velocity (cm/s)
RT1F	16.27	1.59	24.69
RT2F	16.80	1.79	23.84
RT3F	16.49	1.98	24.27
RT4F	15.40	2.19	25.41
RT5F	15.51	2.37	24.82

3. NUMERICAL SIMULATION

The numerical model aimed to cross-check the experimental results. Therefore, the numerical simulations used the same input parameters of the net cage model listed in Table 1. The subsequent sections will provide a brief introduction to the numerical method.

3.1 Regular wave with a uniform current

The numerical domain was considered herein as a three-dimensional (3D) space with a uniform bottom and adopted a superposition principle of linear velocity potential functions to represent a flow field, including a steady uniform current and a regular progressive wave, given as

$$\phi(x,y,z,t) = -\left(U_x x + U_y y\right) + \frac{Hg}{2\omega_e}\frac{\cosh k\,(h+z)}{\cosh k\,h}\cos\left(k_x x + k_y y - \omega t\right), \tag{1}$$

where U_x and U_y are the components of a uniform current in the x and y directions, respectively; (x, y, z) is a position coordinate; H is the wave height; ω is the wave angular frequency; $\omega_e = \omega - (k_x U_x + k_y U_y)$ is referred to as the i-th apparent wave angular frequency; k is the wave number; $k_x = k\,cos\,\alpha$ is the component of the wave number in the x-direction; $k_y = k\,sin\,\alpha$ is the component of the wave number in the y-direction, where α is an apparent angle defined as the angle between the regular wave and current directions; g is gravity; t is time; and h is the water depth. The water surface elevation η is calculated as

$$\eta = \frac{H}{2}\sin\left(k_x x + k_y y - \omega t\right), \tag{2}$$

The correspondent dispersion relation for the wave and current coexisted field is given as

$$\omega_e^2 = gk\tanh kh, \tag{3}$$

We obtain a 3D velocity field, where velocity is defined as $\boldsymbol{V} = -\nabla\phi$, by taking the derivative of Eq. (1) with respect to (x, y, z):

$$\begin{cases} u = U_x + \dfrac{Hgk_x \cosh k\,(h+z)}{\omega_e \cosh k\,h} \sin\left(k_x x + k_y y - \omega t\right), \\ v = U_y + \dfrac{Hgk_y \cosh k\,(h+z)}{2\omega_e \cosh k\,h} \sin\left(k_x x + k_y y - \omega t\right), \\ w = -\dfrac{Hgk \sinh k\,(h+z)}{2\omega_e \cosh k\,h} \cos\left(k_x x + k_y y - \omega t\right), \end{cases} \tag{4}$$

Similarly, the local accelerations for the 3D field are obtained as follows by taking the derivative of Eq. (4) with respect to t:

$$\begin{cases} \dfrac{\partial u}{\partial t} = -\dfrac{\omega Hgk_x \cosh k\,(h+z)}{\omega_e \cosh k\,h} \cos\left(k_x x + k_y y - \omega t\right), \\ \dfrac{\partial v}{\partial t} = -\dfrac{\omega Hgk_y \cosh k\,(h+z)}{2\omega_e \cosh k\,h} \cos\left(k_x x + k_y y - \omega t\right), \\ \dfrac{\partial w}{\partial t} = -\dfrac{\omega Hgk \sinh k\,(h+z)}{2\omega_e \cosh k\,h} \sin\left(k_x x + k_y y - \omega t\right), \end{cases} \tag{5}$$

Velocity and acceleration fields are then applied to the Morison equation based on the lumped mass method to obtain the hydrodynamic forces acting on the net cage (Huang et al., 2007).

3.2 Equation of motion

The Morison equation is commonly used to calculate the hydrodynamic force acting on submerged structures in waves and currents. It is based on the principle that the force exerted by a fluid on a structure can be decomposed into two components: the drag force and the added mass force. The drag force is proportional to the relative velocity between the fluid and the structure, while the added mass force is proportional to the acceleration of the fluid caused by the motion of the structure.

In this study, the deformable components of the net cage model, i.e., the fish nets and the mooring lines, were modeled using the lumped mass method, where the components were divided into small elements to simplify the numerical calculations. The Morison equation was then applied to each element to calculate the hydrodynamic forces acting on them. The rigid parts of the net cage, i.e., the nondeformable floating collar and the tube sinker, were also modeled using the Morison equation.

By dividing the net cage model into deformable and rigid components and appropriately applying the Morison equation, the hydrodynamic forces acting on the net cage system in regular waves and uniform currents were accurately calculated in the numerical simulations.

In this model, each deformable component comprised several elements and nodes assigned with numbers. For each element, the external forces were calculated, and the resultant force was evenly distributed among the corresponding nodes. Thus, each node contained the lumped mass of all neighboring elements and their corresponding forces. Its equation of motion is expressed as follows:

$$\sum_{j=1}^{N_e} m_j \ddot{\boldsymbol{x}}_i = \sum_{j=1}^{N_e} \boldsymbol{F}_{D_j} + \boldsymbol{F}_{I_j} + \boldsymbol{F}_{B_j} + \boldsymbol{F}_{W_j} + \boldsymbol{F}_{T_j}, \tag{6}$$

where subscript i denotes the node number; j denotes the neighboring elements associated with i-th node; N_e represents the total number of neighboring elements; m_j is the mass matrix; $\boldsymbol{x}$ is the position vector; and $\boldsymbol{F}_{D_j}$, $\boldsymbol{F}_{I_j}$, $\boldsymbol{F}_{B_j}$, $\boldsymbol{F}_{W_j}$, and $\boldsymbol{F}_{T_j}$ represent the vectors of the drag, inertia, buoyant, gravity, and tension forces, respectively, acting on j-th element. Details on the external force modeling of the cage components can be found in the previous works of Huang et al. (2006 and 2007).

The motion of the rigid components of the net cage system, including the floating collar and the tube sinker, can be resolved by the rigid body motion with six degrees of freedom (DOF) in a 3D space. The three translation motions can be expressed as

$$\begin{cases} \ddot{x}_G = \dot{y}_G\omega_3 - \dot{z}_G\omega_2 + \dfrac{1}{m_G}\displaystyle\sum_{k=1}^{N_n} F_{x_k}, \\ \ddot{y}_G = \dot{z}_G\omega_1 - \dot{x}_G\omega_3 + \dfrac{1}{m_G}\displaystyle\sum_{k=1}^{N_n} F_{y_k}, \\ \ddot{z}_G = \dot{x}_G\omega_2 - \dot{y}_G\omega_1 + \dfrac{1}{m_G}\displaystyle\sum_{k=1}^{N_n} F_{z_k}, \end{cases} \tag{7}$$

and the three rotational motions can be expressed as

$$\begin{cases} \dot{\omega}_1 = -\dfrac{1}{I_1}(I_3 - I_2)\omega_2\omega_3 + \dfrac{1}{I_1}\displaystyle\sum_{k=1}^{N_n} M_{1_k}, \\ \dot{\omega}_2 = -\dfrac{1}{I_2}(I_1 - I_3)\omega_3\omega_1 + \dfrac{1}{I_2}\displaystyle\sum_{k=1}^{N_n} M_{2_k}, \\ \dot{\omega}_3 = -\dfrac{1}{I_3}(I_2 - I_1)\omega_1\omega_2 + \dfrac{1}{I_3}\displaystyle\sum_{k=1}^{N_n} M_{3_k}, \end{cases} \tag{8}$$

where subscripts 1 to 3 and x, y, and z correspond to the body and global coordinate systems, respectively; (x_G, y_G, z_G) are the coordinates of the center of gravity; $(\omega_1, \omega_2, \omega_3)$ are the angular velocities along the principal axes; m_G is the body mass; $(F_{x_k}, F_{y_k}, F_{z_k})$ and $(M_{1_k}, M_{2_k}, M_{3_k})$ are the components of the resultant forces and moments acting at the lumped mass node k; N_n is the number of nodes in the body; and (I_1, I_2, I_3) are the principal moments of the rigid body inertia. For the floating collar and the tube sinker, $I_1 = 0.5m_GR^2$, $I_2 = 0.5m_GR^2$, and $I_3 = m_GR^2$, where R is the rigid body radius.

We can obtain a solution with a short time increment by applying the fourth-order Runge–Kutta method to the equation of motion in the net cage system [Eqs. (6)–(8)]. The path of each node, including the mass center of the rigid body, is accordingly depicted herein. By computing the neighboring node

distance, the tension force of the flexible part is obtained and used as the input tension data for the next time step until the required time interval is spent.

In this work, the net cage model was divided into 844 elements and 791 nodes, and the time step for the numerical integration was 0.0001 s. The number of nodes and elements and the time step in the preliminary stage were determined through time domain convergence tests. The total number of elements on the fish net was 480, including 24 and 20 in the circumferential and depth direction of the net, respectively. The element on each mooring line was 25.

3.3 Force on the net

The hydrodynamic forces on the netting were calculated using the screen model (Huang et al., 2006; Kristiansen and Faltinsen, 2012). In the algorithm, the whole netting structure was divided into many small screens (or elements), with each screen containing many mesh twines. The tension, buoyancy, and gravity forces acting on each screen represented the sum of the forces exerted on the twines in the screen. Finally, the total forces on the screen were assumed to be evenly distributed among the nodes. The drag $C_D(\beta)$ and lift $C_L(\beta)$ coefficients depended on the flow attack angle β. They can be determined using the experimental results by Løland (1991).

$$C_D(\beta) = 0.04 + (-0.04 + 0.33S_n + 6.54{S_n}^2 - 4.88{S_n}^3)\, cos(\beta), \tag{9}$$

$$C_L(\beta) = (-0.05S_n + 2.3{S_n}^2 - 1.76{S_n}^3)\, sin(2\beta), \tag{10}$$

The solidity ratio S_n is the ratio between the area covered by the twines in the screen and the total area of the screen. It is expressed as follows for a knotless net:

$$S_n = \frac{2D}{\lambda} - \left(\frac{D}{\lambda}\right)^2, \tag{11}$$

where D is the twine diameter and λ is half of the mesh size. The fluid particle velocity was slightly retarded after entering the net cage. This phenomenon is known as the shielding effect. A velocity reduction coefficient of 0.85 was adopted for the rear part of the nets (Løland, 1991).

3.4 Simulation of the mooring line failure

All anchor points in the intact mooring state were considered as fixed nodes to simulate the net cage dynamics. To do that, the equation of motion of all anchor points was set to $\ddot{\boldsymbol{x}}_k = 0$. It is to ensure all anchor points will not move. In contrast, anchor point #1 was changed to a free node and allowed to move freely according to the equation of motion to simulate the mooring line failure (Yang et al., 2020). In the other word, we can lift the restriction of the anchor point ($\ddot{\boldsymbol{x}}_k = 0$), then it will move freely in the next time step depending on the external forces as shown in Eq. (6). In this study, a predetermined time of 20 s after the start of the simulation was set as the moment of failure occurrence. The experimental setup showed a total simulation time of 60 s. The results were then compared with those in the experiments.

4. RESULTS AND DISCUSSIONS

4.1 Experimental results

Figure 4 shows the time histories of tension in the upstream two load cells in the RH3F test case listed Table 3. At 30 s of cutting the line, the tension in Line 1 drops rapidly to zero while the tension in Line 2 increases dramatically. The results indicated that one mooring line failure can lead to a significant increase of mooring load on its adjacent line by more than 50%.

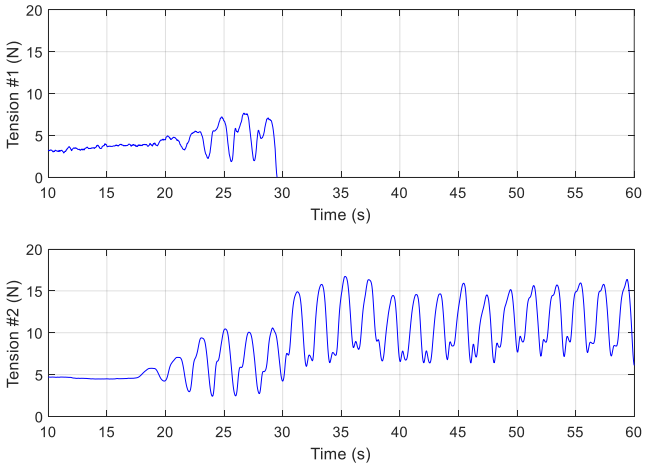

Figure 4. Time history of load cells in the RH3F case.

Figure 5 shows the time histories of the roll, pitch, and yaw motions of the floating collar for the RH3F test cases listed in Table 3. In the experiment, the wave train was propagated in the *x*-direction and the mooring system of the net cage is symmetrical. After 20 s, the wave train reached the net cage and forced the floating collar to pitch significantly, while the roll and yaw were small. After cutting the line at 30 s, the yaw motion increased rapidly up to 15 degrees, with little change in roll and pitch.

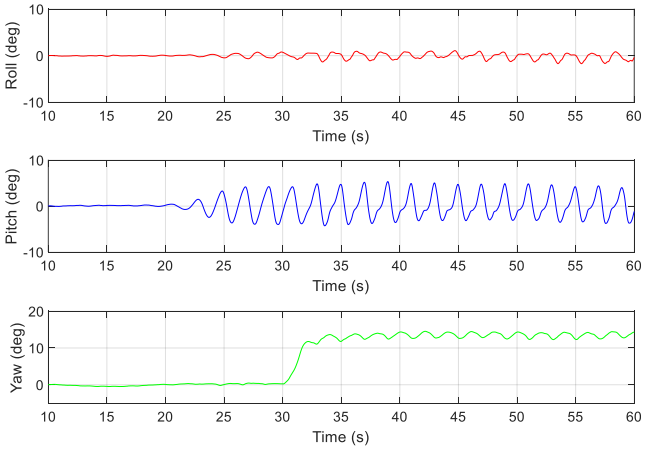

Figure 5. Time history of roll, pitch, and yaw of the floating collar in the RH3F case.

4.2 Validation of the numerical simulation

Figure 6 compares the mooring tension in Line 2 between the experiment and the simulation under intact and failed mooring conditions for cases RH3I and RH3F. In the intact condition, the comparison between the experiment and the simulation was in good agreement. In the failed condition, the numerical simulation overestimated the mooring loads, especially after the second peak (about 33 s). The difference could be that the mooring system in the experiment is not perfectly symmetric, and the wave-structure interaction was ignored in the numerical simulation. Overall, the present numerical model can satisfactorily predict the dynamic response of the sudden mooring line failure on the net cage.

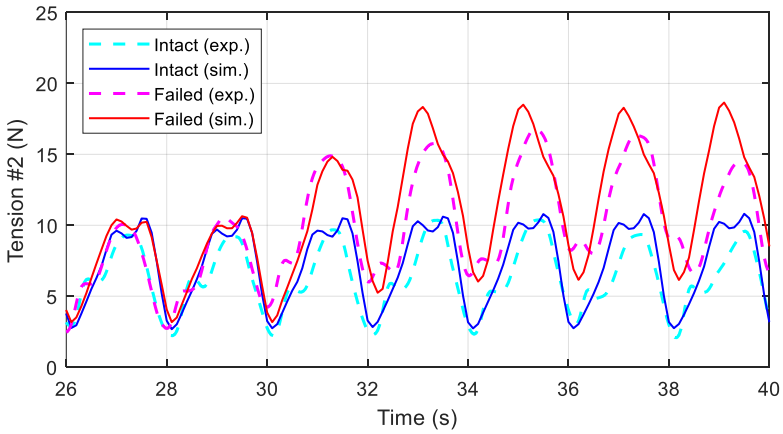

Figure 6. Comparison of mooring tension in Line 2 for cases RH3I and RH3F.

4.3 Effects of wave heights on the mooring tension under the failure

Figure 7 compares the maximum mooring tension in Line 2 between the experiment and the simulation under intact and failed mooring conditions with different wave heights. The maximum value was obtained between 30 s and 40 s, see Figure 6. The increase in tension in Line 2 was proportional to the wave height for both intact and failed conditions. Also, the comparative results were in good agreement.

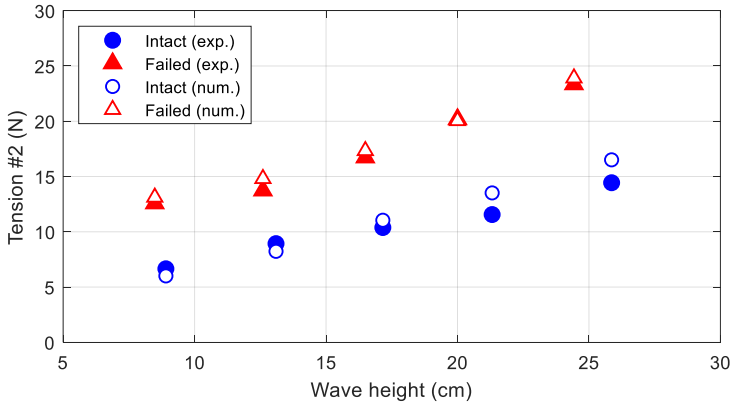

Figure 7. Comparison of the maximum tension in Line 2 under intact and failed conditions with different wave heights.

4.4 Effects of wave periods on the mooring tension under the failure

Figure 8 compares the mooring tension in Line 2 between the experiment and the simulation under intact and failed mooring conditions with different wave periods. In the experiment, the tension in line 2 increased with the wave period in both intact and failed conditions. However, the trend in the simulation results is not clear. The discrepancy can be seen in the low wave periods of 1.6 s and 1.8 s, where the greater wave steepness exists. This suggests that the error may be due to the nonlinear wave effects.

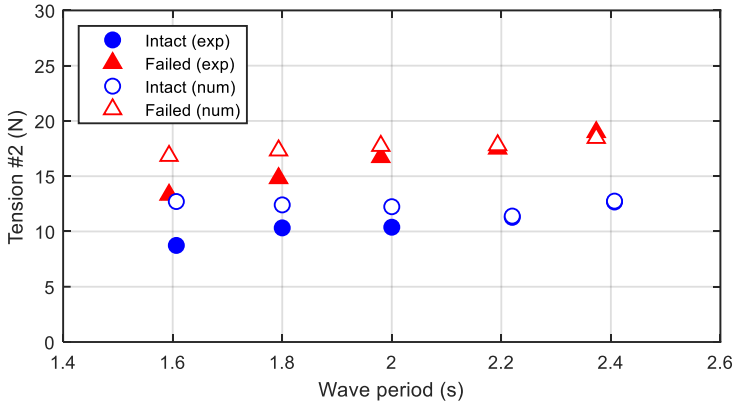

Figure 8. Comparison of the maximum tension in Line 2 under intact and failed conditions with different wave periods.

4.5 Effects of wave heights on the yaw motion under the failure

Figure 9 compares the maximum value of the yaw motion in the test cases of different wave heights listed in Table 2 and Table 3. In the intact condition, the yaw motions are small in both the experiment and the simulation. In the failed condition, the yaw motions are significantly increased in both experiments and simulations. The experimental value is between 13.8 degrees and 16.5 degrees, the simulated value is between 5.2 degrees and 6.4 degrees. The experimental value is obviously larger, which should be due to the fact that the mooring lines in the experiment were not fully tensioned and symmetrical, as explained by Tang et al. (2022a). In addition, the maximum yaw after failure was slightly proportional to the wave height.

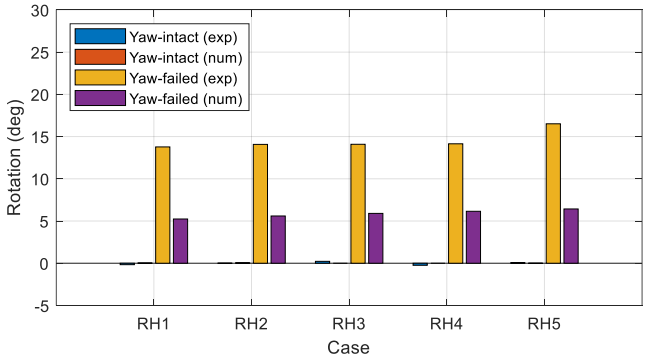

Figure 9. Comparison of yaw motion under different wave height

4.6 Effects of wave periods on the yaw motion under the failure

Figure 10 shows the comparison of the maximum value of the yaw motion in the test case of changing the wave period as listed in Table 4 and Table 5. In the intact condition, there is no obvious yaw rotation in the experiment and simulation. In the failed condition, the yaw motion of both has increased significantly, and the experimental value is between 14.8 degrees and 16.1 degrees, and the simulated value is between 5.8 degrees and 6.0 degrees. The experimental value is obviously larger, and the reason for the error is the same as mentioned above. However, the relationship between the yaw motion and the wave period after the failure is not significant.

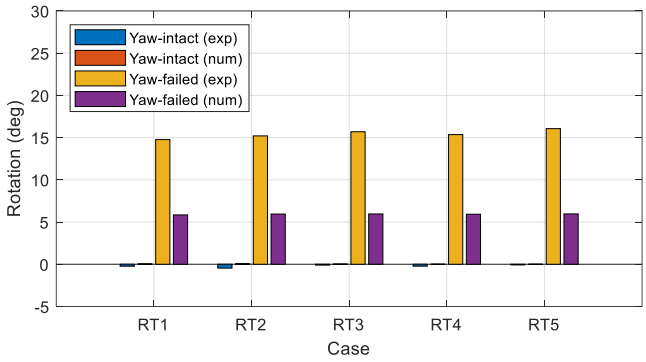

Figure 10. Comparison of yaw motion under different wave period

5. CONCLUSIONS

In this study, the net cage was tested in a wave tank to investigate the dynamic response due to sudden mooring line failure in regular waves and uniform current. The effects of wave height and wave period on the dynamic response were compared. A numerical model specially designed for the model test was used for cross-validation. According to the results, the following conclusions and suggestions can be made.

First, the mooring line failure induced mooring loads on the remaining line and the yaw motion of the floating collar are very significant. Second, wave height plays a more critical role than wave period in increasing mooring loads in both intact and failed conditions. Third, wave effects on yaw motion are less important than mooring loads. Also, the numerical model can predict the dynamic response due to sudden mooring line failure acceptably. Finally, due to the significant pattern of dynamic response after failure, the mooring line failure event could be detected by artificial neural network technology in future studies.

ACKNOWLEDGEMENTS

This work received funds from the National Science and Technology Council of Taiwan (grant no. 109-2222-E-006-003-MY2 and 110-2221-E-006-166-MY2). The authors are especially grateful to the Reviewers for their help in improving the article.

AUTHOR'S CONTRIBUTION

HJT designed the experiments, processed the data, and wrote the first draft of the manuscript. RYY supervised and coordinated the project. HCY undertook the experiments and processed the data. All authors edited and approved the manuscript.

REFERENCES

Cheng, H., Li, L., Ong, M.C., Aarsæther, K.G. and Sim, J. (2021). Effects of mooring line breakage on dynamic responses of grid moored fish farms under pure current conditions. Ocean Engineering, 237, 109638.

Hou, H.M., Liu, Y., Dong, G.H. and Xu, T.J. (2022). Reliability assessment of mooring system for fish cage considering one damaged mooring line. Ocean Engineering 257, 111626.

Huang, C.C., Tang, H.J. and Liu, J.Y. (2006). Dynamical analysis of net cage structures for marine aquaculture: Numerical simulation and model testing. Aquacultural Engineering, 35(3), 258–270.

Huang, C.C., Tang, H.J. and Liu, J.Y. (2007). Modeling volume deformation in gravity-type cages with distributed bottom weights or a rigid tube-sinker. Aquacultural Engineering, 37(2), 144–157.

Løland, G. (1991). Current Forces on and Flow through Fish Farms (Doctoral Thesis). The Norwegian Institute of Technology, Trondheim, Norway.

Kristiansen T., and Faltinsen, O.M. (2012). Modelling of current loads on aquaculture net cages. Journal of Fluids and Structures, 34, 218–235.

Kristiansen, T. and Faltinsen, O.M. (2015). Experimental and numerical study of an aquaculture net cage with floater in waves and current. Journal of Fluids and Structures, 54, 1–26.

Tang, H.J., Yeh, P.H., Huang, C.C. and Yang, R.Y. (2020). Numerical study of the mooring system failure of aquaculture net cages under irregular waves and current. Ocean Engineering, 216, 108110.

Tang, H.J., Yang, R.Y. and Yao, H.C. (2021). Experimental and numerical investigations of a mooring line failure of an aquaculture net cage subjected to currents. Ocean Engineering, 238, 109707.

Tang, H.J., Yao, H.C. and Yang, R.Y. (2022a). Experimental and numerical studies on successive failures of two mooring lines of a net cage subjected to currents. Ocean Engineering, 266, 113243.

Tang, H.J., Chiang, W.S. and Nan, F.H. (2022b). Engineering feasibility assessment of cage aquaculture in offshore wind power generation areas in Taiwan. Sustainability 14(18), 11705.

Tang, H.J., Yang, R.Y. and Yao, H.C., (2023). Experimental and numerical study on the hydrodynamic behaviors of mooring line failure on a net cage in irregular waves and currents. Frontiers in Marine Science, 10, 1122855.

Yang, R.Y., Tang, H.J. and Huang, C.C. (2020). Numerical modeling of the mooring system failure of an aquaculture net cage system under waves and currents. IEEE Journal of Oceanic Engineering, 45(4), 1396-1410.